SynBio

MDPI

Communication

First Recombinant Expression, Purification, and Film Formation of a Single Solitary Bee Silk Protein from *Osmia lignaria*

Oran Wasserman, Kristin K. Durrant, Jackson J. Morley, Paula E. Oliveira, Mallory R. Wootton, Brianne E. Bell, Ethon D. Van Noy, Randolph V. Lewis and Justin A. Jones *

Department of Biology, Utah State University, Logan, UT 84322, USA; kristin.durrant@usu.edu (K.K.D.); jackson.morley27@gmail.com (J.J.M.)
* Correspondence: justin.a.jones@usu.edu; Tel.: +1-(435)-797-9292

Abstract

Solitary bees account for most described bee species worldwide, with many spinning silk fibers to form protective cocoons during development; however, solitary bee silk proteins remain largely unexplored in recombinant systems and biomaterial fabrication. Here, we report the first recombinant expression and biomaterial formation from a solitary bee silk protein. *Osmia lignaria* silk fibroin 2 (OligF2) was expressed in *Escherichia coli* BL21(DE3) using an expression and purification scheme adapted from a recombinant hagfish intermediate filament (rHIF) workflow, yielding 0.34 g/L at ~70% purity. The purified OligF2 protein was cast into films at 0.75% and 1% (*w*/*v*). Fourier-transform infrared attenuated total reflectance (FTIR-ATR) analysis estimated higher β-sheet content in 0.75% films (50.3%) than in 1% films (42.3%). Mechanical testing yielded elastic moduli of 7.83 ± 2.73 MPa and 6.80 ± 1.89 MPa for the 0.75% and 1% films, respectively. These results establish the first recombinant production and biomaterial formation of a solitary bee silk protein, providing a foundation for exploring this class of recombinant proteins for the development of tunable biomaterials.

Keywords: *Osmia*; recombinant; biomaterial; expression; inclusion body

1. Introduction

Silk production is widespread among arthropods and has evolved independently across multiple lineages, including spiders, lepidopterans, and various insect groups [1,2]. Recombinant expression of silk proteins has emerged in recent years as a viable approach for producing versatile biomaterials for diverse applications [3–5]. Within Hymenoptera, recombinant production of silk proteins has focused on social species such as hornets and honeybees [6–9]. Notably, aculeate silk fibers are typically composed of four small, homologous proteins that form a tetrameric coiled-coil structure [2]. The four *Apis mellifera* fibroins (AmelF1–4) proteins have been expressed in *Escherichia coli* at high yields [8]. In addition, it was demonstrated that a single *A. mellifera* silk protein (AmelF3) can be processed into films, fibers, and sponges [10–12].

Solitary bees comprise the majority of bee diversity [13]. Some species, such as those in the genus *Osmia*, spin silk during development to construct protective cocoons [13–17], yet their silk proteins have not been recombinantly expressed or used in protein-based biomaterial development. Our lab has previously characterized the mechanical properties of *O. lignaria* silk fiber and cocoon puncture resistance [14,15]. Additionally, recent advances from our lab have established a robust expression and purification platform for

Check for updates

Received: 3 April 2026
Revised: 3 May 2026
Accepted: 11 May 2026
Published: 14 May 2026

Copyright: © 2026 by the authors. Licensee MDPI, Basel, Switzerland. This article is an open access article distributed under the terms and conditions of the Creative Commons Attribution (CC BY) license.

recombinant hagfish intermediate filament (rHIF) proteins, including rHIF-α and rHIF-γ, achieving yields of ~8 g/L in *E. coli* [16–18]. The increasing availability of annotated *Osmia* genomes [19–24] creates an opportunity to systematically explore solitary bee silk proteins as a largely untapped design space for recombinant biomaterials. However, the lack of established recombinant production workflows has limited access to these systems.

In this study, we present the recombinant expression, purification, and biomaterial formation of a solitary bee silk protein. Given that aculeate silk fibroins share coiled-coil architecture and aggregation-prone expression behavior with rHIF proteins, we evaluated whether the rHIF inclusion-body purification workflow [16–18] could enable scalable production of OligF2. All three currently annotated *O. lignaria* silk fibroins (OligF2–4) were screened in shake flask cultures, and, because a single *A. mellifera* fibroin is sufficient for biomaterial formation [10–12], OligF2 was selected for scale-up based on the highest expression yield observed. The OligF2 gene construct was codon optimized, cloned into pET19k, and expressed in *E. coli* BL21(DE3). Film formation and mechanical characterization were performed using established solvent-casting and hydration protocols [25].

2. Results

2.1. Recombinant Expression and Purification

To evaluate whether the rHIF inclusion-body purification workflow could recover OligF2, the protein was expressed in *E. coli* BL21(DE3) using rHIF-derived expression conditions. SDS-PAGE Coomassie (Figure 1A) and Western blot (Figure 1B) analyses of the purified protein pellet showed a band at the expected OligF2 molecular weight (~35 kDa), with rHIF-α (~70 kDa) included for comparison. Based on ImageJ 1.54s analysis, purity was estimated at ~70% (Figure 1A). The final purified protein pellet yield, calculated from the overall bioreactor volume, was 0.34 g/L.

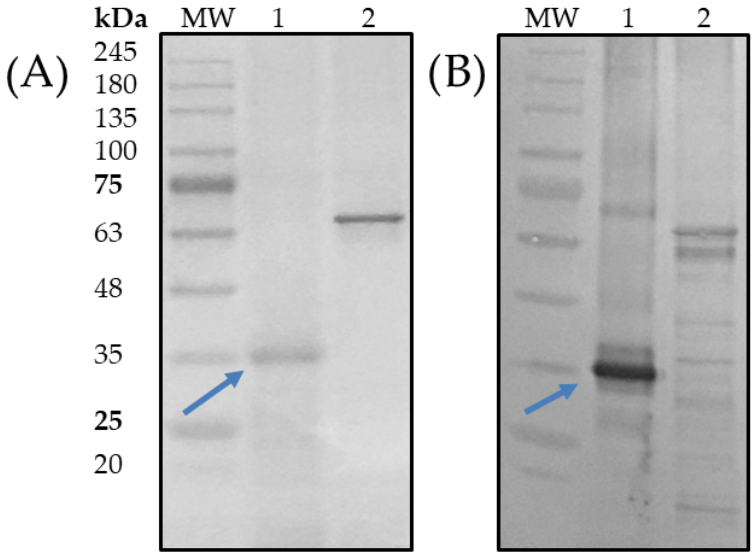


Figure 1. Analysis of purified OligF2. (**A**) Coomassie-stained SDS-PAGE. (**B**) Western blot probed with anti-His antibody. MW: Tris-Glycine 4–20% pre-stained protein ladder; Lane 1: OligF2; Lane 2: rHIF-α (positive control). Blue arrow indicates the target OligF2 band (~35 kDa).

2.2. Film Formation and Characterization

To assess the film-forming capacity and secondary structure of purified OligF2, the lyophilized protein pellet was dissolved in 72.75% formic acid and cast into transparent films at 0.75% *w*/*v* and 1% *w*/*v* (Figure S1A,B). FTIR-ATR spectroscopy was used to characterize secondary structure. The normalized amide I band for both film concen-

trations (Figure 2A) showed a prominent feature near ~1652 cm^{-1} and a shoulder near ~1621 cm^{-1}. Gaussian deconvolution of the amide I region (1600–1700 cm^{-1}) revealed three peaks corresponding to β-sheet (~1621 cm^{-1}), α-helix/coiled-coil (~1652 cm^{-1}), and antiparallel β-sheet (~1697 cm^{-1}) structures for both the 0.75% *w*/*v* (Figure 2B) and 1% *w*/*v* (Figure 2C) films [26–30]. β-sheet content was calculated from the sum of the ~1621 cm^{-1} and ~1697 cm^{-1} peaks. Based on relative peak areas, the 0.75% *w*/*v* films were estimated to contain 50.3% β-sheet and 49.7% α-helix/coiled-coil content, while the 1% *w*/*v* films were estimated to contain 42.3% β-sheet and 57.7% α-helix/coiled-coil content (Figure 2D). Gaussian fits yielded R^2 values of 0.989 for both film concentrations.

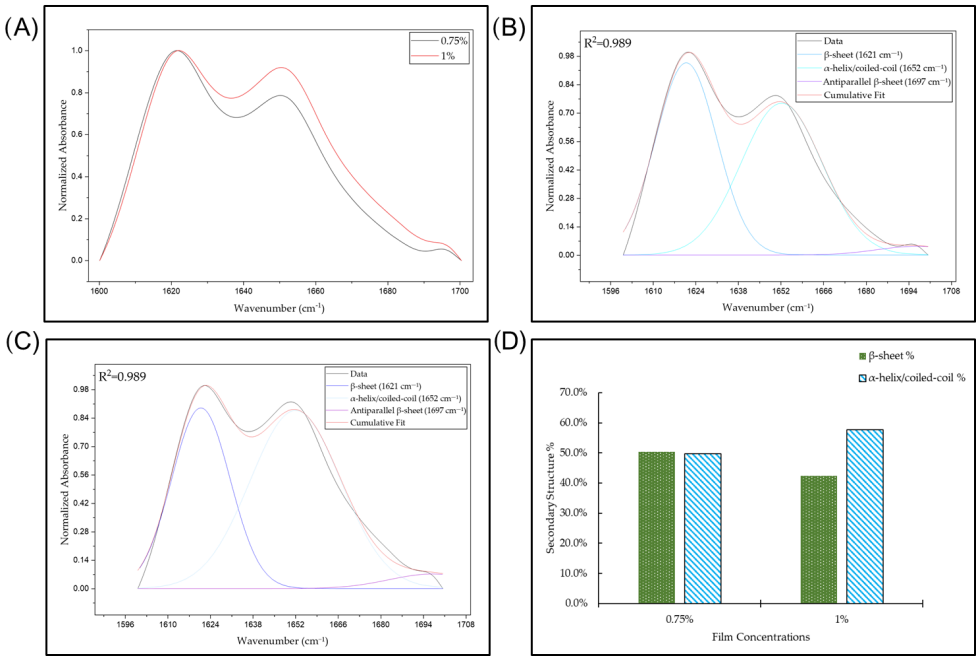


Figure 2. OligF2 film characterization. (**A**) Normalized amide I spectra of 0.75% *w*/*v* (black) and 1% *w*/*v* (red) films. (**B**,**C**) Gaussian deconvolution of the amide I region for 0.75% (**B**) and 1% (**C**) films showing β-sheet (1621 cm^{-1}), α-helix/coiled-coil (1652 cm^{-1}), and antiparallel β-sheet (1697 cm^{-1}) peaks. R^2 = 0.989 for both fits. (**D**) Quantification of β-sheet and α-helix/coiled-coil content for 0.75% *w*/*v* and 1% *w*/*v* films.

Stress–strain curves for individual OligF2 film samples (n = 9 per concentration) within the linear region used for elastic modulus calculations are shown in Figure 3. All samples exhibited a linear elastic region between 0.3 and 0.7 MPa, with $R^2 > 0.97$. The 0.75% *w*/*v* films exhibited steeper slopes than the 1% *w*/*v* films, correlating with higher elastic modulus values. Additionally, the 0.75% *w*/*v* films displayed greater mechanical variability, reflected by a wider distribution of strain values at equivalent stress (Figure 3). Elastic moduli of 7.83 ± 2.73 MPa and 6.80 ± 1.89 MPa were obtained for the 0.75% *w*/*v* and 1% *w*/*v* films, respectively (Figure 3). No statistically significant difference was observed between concentrations (t = 0.93, p = 0.366; 95% CI for the mean difference: −1.34 to 3.40 MPa; Cohen's d = 0.44). Because the films did not break within the instrument's deflection limits, ultimate tensile strength, elongation at break, and toughness were not obtained, and the reported values reflect small-strain elastic behavior only.

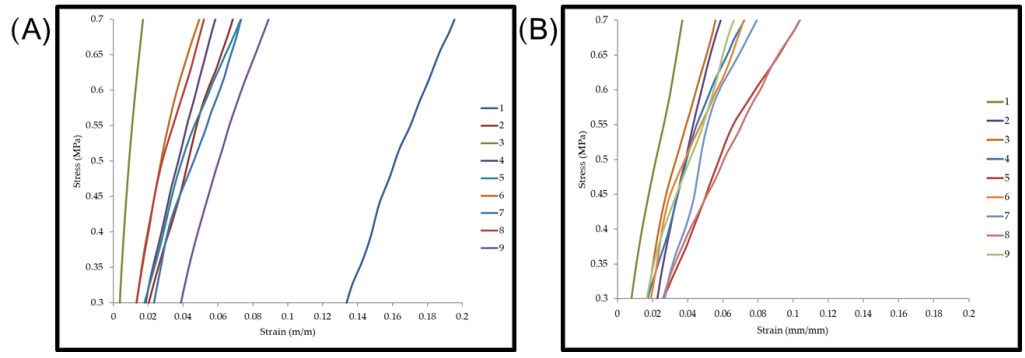


Figure 3. Stress–strain curves for hydrated OligF2 films within the linear region (0.3–0.7 MPa) used for elastic modulus calculation: (**A**) 0.75% *w*/*v* and (**B**) 1% *w*/*v* films (*n* = 9 per concentration from three independently cast films).

3. Discussion

Recombinant structural proteins driven by strong T7 promoters commonly accumulate in the insoluble fraction in *E. coli* [31], and OligF2 exhibited similar aggregation behavior. Importantly, the rHIF-derived purification workflow, including pI-adjusted wash buffers and organic solvent rinses, enabled recovery of OligF2 at 0.34 g/L without extensive process redesign. OligF2 yield falls within the range reported for social hymenopteran silk proteins (Table 1), comparable to *Vespa simillima* (0.16–0.33 g/L) and within the lower range of *A. mellifera* fibroins (0.2–2.5 g/L), while exceeding *A. cerana* (0.01–0.06 g/L) but below *A. dorsata* (1.6–2.6 g/L) [6–9]. The recovered protein pellet was estimated to be approximately 70% pure by densitometric analysis, with the dominant band corresponding to OligF2. Residual contaminants may contribute to the observed film formation and properties. Additional chromatographic polishing may increase the recovered protein purity and enable more refined structure–property investigations in future studies.

Table 1. Expression yields of OligF2 compared to other recombinant hymenopteran silk proteins, all expressed in *E. coli*. Ranges for other species represent yields across individual fibroin proteins. The fraction column indicates whether the protein was purified from the soluble or insoluble (inclusion body) fraction.

Protein	Species	Yield (g/L)	Fraction	Reference
OligF2	*Osmia lignaria*	0.34	Insoluble	This work
ABS1–4	*Apis cerana*	0.01–0.06	Soluble	[6]
AdorF1–4	*Apis dorsata*	1.6–2.6	Insoluble	[7]
AmelF1–4	*Apis mellifera*	0.2–2.5	Insoluble	[8]
Vssilk1–4	*Vespa simillima*	0.16–0.33	Insoluble	[9]

Although rHIF proteins and hymenopteran silk fibroins differ in sequence and native function, both contain coiled-coil-forming domains and exhibit aggregation during heterologous expression [16,32]. The successful recovery of OligF2 using an inclusion-body purification workflow originally optimized for rHIF proteins suggests that the strongly denaturing, solvent-assisted wash conditions used here are compatible with at least one aggregation-prone coiled-coil silk fibroin. While broader applicability remains to be tested across additional protein systems, these findings demonstrate that recombinant production of OligF2 can be achieved without extensive downstream redesign. Whether this workflow extends to other solitary bee silk proteins remains an open question for future work.

The ability to recombinantly access solitary bee silk proteins expands the available sequence space for engineering protein-based biomaterials. Given the diversity of solitary bee species and their silk compositions, this approach enables systematic exploration

of sequence–structure–property relationships in a class of materials that has remained largely inaccessible.

OligF2 belongs to the family of aculeate silk fibroins characterized by predicted coiled-coil domains and conserved heptad repeat motifs [2,33], which in social hymenopterans assemble into tetrameric coiled-coil structures [8,34,35]. Consistent with the demonstrated capacity of a single fibroin (AmelF3) to form biomaterials independently [10–12], the successful film formation observed for OligF2 extends single-fibroin biomaterial formation to a solitary bee silk protein. While naturally occurring *O. lignaria* silk is likely to involve multicomponent interactions, the present results demonstrate that OligF2 adopts secondary-structure features consistent with structured protein film formation when processed in isolation.

The presence of both α-helix/coiled-coil and β-sheet features in the OligF2 films is consistent with the predicted coiled-coil architecture of aculeate silk fibroins and suggests partial retention or reorganization of native structural motifs during solvent casting. The higher β-sheet content in the 0.75% w/v films relative to the 1% w/v films (50.3% vs. 42.3%) suggests concentration-dependent molecular organization during film formation. The mechanistic basis of this trend warrants further investigation in future studies. The asymmetric amide I profile observed in OligF2 films, with visually distinguishable features in the β-sheet (~1621 cm^{-1}) and α-helix/coiled-coil (~1652 cm^{-1}) regions prior to deconvolution, is consistent with established FTIR studies of proteins containing mixed secondary structures. Byler and Susi demonstrated that protein amide I bands typically consist of multiple overlapping components at characteristic frequencies [36]. Mello et al. hypothesized the coexistence of α-helix and β-sheet conformations in the cocoon silk of *Lithurgus chrysurus*, another solitary bee in the family Megachilidae [26]. However, because coiled-coil α-helices can produce amide I bands that overlap with β-sheet assignments [37], the secondary structure content reported here should be interpreted as estimates pending further characterization using complementary techniques. Accordingly, future work incorporating methods such as circular dichroism or X-ray scattering will be required to further resolve structural contributions [31,35].

The hydrated OligF2 films did not break during mechanical testing due to instrument deflection limits. Accordingly, ultimate tensile strength, elongation at break, and toughness were not obtained, and the reported values reflect small-strain elastic behavior under hydrated conditions only. The 0.75% w/v films (7.83 ± 2.73 MPa) exhibited a higher elastic modulus than the 1% w/v film strips (6.80 ± 1.89 MPa), although the difference was not statistically significant. The 0.75% w/v films also exhibited higher estimated β-sheet content. While the established relationship between β-sheet structure and mechanical stiffness in silk-based biomaterials [38] would predict such a trend, the present comparison is descriptive rather than statistically supported. The elastic moduli of hydrated OligF2 films are lower than those reported for hydrated regenerated silk fibroin films (19–22 MPa) [39]. These values place OligF2 films within the modulus range typical of hydrated protein-based biomaterials used for soft tissue scaffolds [25,40–42]. Future studies using higher-force instrumentation will be required to characterize ultimate tensile strength, elongation at break, and toughness. Additional work investigating the effects of post-formation treatments, crosslinking strategies, protein concentration, or the incorporation of other fibrous proteins, such as rHIF, on OligF2 mechanical properties will be necessary to tailor these biomaterials for specific applications. The demonstrated compatibility between OligF2 and rHIF-derived processing workflows also raises the possibility of hybrid or blended systems that combine rHIF proteins with hymenopteran silk fibroins to further tune mechanical and functional properties.

4. Materials and Methods

4.1. Gene Identification and Molecular Cloning

All three currently annotated silk fibroins in the *O. lignaria* genome (OligF2–4; a fourth fibroin has not been identified) were codon-optimized for expression in *E. coli*, synthesized by GeneArt (Thermo Fisher, Madison, WI, USA), and cloned into the pET19k vector at the NdeI and BamHI (New England Biolabs, Ipswich, MA, USA) restriction sites using standard molecular biology techniques as previously described [19] (Figure S2). Physicochemical properties and amino acid composition were calculated using ExPASy ProtParam (SIB Swiss Institute of Bioinformatics) and SnapGene 8.2.2 (Figure S3; Table S1). The pET19k containing the OligF2–4 constructs was transformed into *E. coli* BL21(DE3) (New England Biolabs) for recombinant protein expression.

4.2. Recombinant Expression and Purification

Initial shake flask cultures were used to validate protein expression. Starter cultures were grown overnight in LB medium with kanamycin (100 µg/mL) at 37 °C with shaking at 225 rpm. Expression was performed in 100 mL shake flask cultures induced with 1 mM IPTG at an OD_{600} of ~0.6. SDS-PAGE and Western blot analysis indicated that OligF2–4 accumulated in the insoluble fraction as inclusion bodies. Expression levels were assessed by SDS-PAGE and Western blot, and OligF2 (Gene ID 117607400; RefSeq XP_034186942.1) was selected for scale-up based on the highest expression yield observed. OligF2 has broad ortholog representation across Hymenoptera (13 species), a molecular weight of 34.9 kDa (Figure S3), and amino acid composition similar to other aculeate silk proteins [33].

Expression was then scaled up using a 1 L BioFlo 310 bioreactor (Eppendorf, Hamburg, Germany). The protocol and media components were consistent with previous work [16], with appropriate volume adjustments. The cell mass was harvested via centrifugation (10,000× *g*, 15 min, 4 °C) and stored at −20 °C until purification [16,17].

The inclusion body purification protocol was adapted from the rHIF-based purification scheme [16–18]. Frozen cell pellets were thawed, resuspended in lysis buffer, and lysed by probe sonication (QSonica, Newtown, CT, USA) on ice. The lysate was centrifuged, and the resulting inclusion body pellets were processed through two wash buffers, a tris-acetate-EDTA–isopropyl alcohol (TAE-IPA) wash, and 50% isopropyl alcohol (IPA) rinses as previously described [16]. Two notable changes were made to the method: (1) dithiothreitol (DTT) was omitted from the wash buffer recipes, as described by Bell et al. [18], and (2) the pH of the wash buffers was adjusted to the OligF2 pI (9.4) (Figure S3). The 50% IPA washes were repeated until the conductivity of the supernatant was below 10 µS/cm. The washed proteins were lyophilized, and the final dry protein amount was recorded. Production yield was calculated as g/L and g/kg. SDS-PAGE was performed using Novex Tris-Glycine WedgeWell 4–20% gradient gels (Invitrogen, Carlsbad, CA, USA). Purity was estimated by SDS-PAGE with Coomassie staining, with densitometry performed using ImageJ 1.54s [16,18]. Western blotting with an anti-histidine antibody was used to confirm the identity of the target protein, with rHIF-α as a positive control [16]; membranes were probed with a mouse monoclonal anti-6X His primary antibody (Rockland Immunochemicals, Limerick, PA, USA) followed by an alkaline phosphatase-conjugated anti-mouse IgG (H + L) secondary antibody (Promega, Madison, WI, USA), both used at manufacturer-recommended dilutions.

4.3. Film Formation and Characterization

Lyophilized OligF2 protein pellet was dissolved in 72.75% formic acid at 0.75% *w*/*v* and 1% *w*/*v*, vortexed, and mixed using a rotisserie mixer for 15 min to solubilize the protein dope solution. The dope solution was centrifuged at 4400× *g* for 15 min to remove

any insoluble material, then spread onto polydimethylsiloxane (PDMS) disks and allowed to dry under restricted airflow for approximately 24 h before peeling the film from the disk (Figure S1A,B) [25]. Film thickness and width were measured using brightfield microscopy (BA310, Motic, Universal City, TX, USA). For each film, three thickness measurements (400× total magnification) were taken and averaged. From each film, several film strips were cut prior to mechanical testing and mounted onto a plastic C-card (Figure S1C). Three width measurements (40× total magnification) were taken and averaged for each film strip. The averaged thickness and width values were used to calculate the cross-sectional area for mechanical stress calculations.

FTIR-ATR spectra were collected using a Thermo Nicolet iS50 spectrometer (Madison, WI, USA) equipped with a built-in diamond ATR module and DLaTGS detector. Spectra were acquired over the 400–4500 cm^{-1} range at 4 cm^{-1} resolution with 50 scans co-added per spectrum. Four spectra per film concentration were baseline corrected, averaged, normalized to maximum amide I absorbance, and deconvolved in the 1600–1700 cm^{-1} region using OriginPro 2025 (OriginLab) [26]. Peak positions were identified from the minima of the second derivative using Savitzky–Golay smoothing (second-order polynomial, 7-point window) and assigned to secondary-structure components based on established protocols for fibrous proteins [17,27,28]. The best absorbance assignments were determined using Gaussian curve fitting with a maximum of 400 iterations and a tolerance of 1×10^{-14}, maximizing R^2 while minimizing the chi-squared statistic. Secondary structure content was calculated from peak areas, with β-sheet content determined from the sum of peaks assigned to β-sheet and antiparallel β-sheet structures, as well as α-helix/coiled-coil content from the corresponding assigned peak.

Mechanical testing was performed using a MicroTester G2 (CellScale, Waterloo, ON, Canada) [25]. Films were cut into 2 mm-wide strips and subjected to a series of ethanol washes (50% and 100% EtOH) followed by hydration in DPBS (−/−) to simulate conditions relevant to potential cell-scaffold applications. Individual film strips were mounted across a custom spacer with a 3 mm gap and 10 mm length, with support towers sufficient to cover the extension limit of the device. Custom clamps were placed on top of each mounting tower to secure the film strip in place. Samples were stretched at 25 µm/s using a 0.5588 mm-diameter tungsten rod (beam length 46–52 mm) until failure, defined as either film fracture or the beam reaching the bottom of the testing gap. Stress–strain curves were generated, and the initial linear portions were used to calculate the elastic modulus. The hydrated films did not break during testing, as the instrument's deflection range was insufficient to fracture the robust films. Therefore, mechanical characterization focused on the elastic modulus calculated from the initial linear region of the stress–strain curves.

Test data were exported to Excel, where the raw force (µN) and tip displacement (µm) were combined with the averaged thickness and width measurements to calculate stress and strain, with adjustments to account for the 3-point bending geometry. For each concentration, a linear region was identified from the stress–strain curves and applied consistently across all samples (n = 9 per concentration). Elastic modulus was calculated as the slope of stress (Pa) versus strain (m/m) within the linear region, and values were converted to MPa by dividing by 10^6. R^2 values verified the linearity of the selected ranges. Statistical analyses were performed using OriginPro 2025 (OriginLab). Normality was assessed using the Shapiro–Wilk test. Elastic modulus values were compared between the two film concentrations using Welch's t-test, with a significance threshold of $\alpha = 0.05$. Values are reported as mean ± standard deviation.

5. Conclusions

Here, we demonstrate that a recombinant production and processing workflow developed for hagfish intermediate filament proteins can be extended to enable scalable expression and biomaterial formation from a solitary bee silk protein, representing the first reported recombinant production of a solitary bee silk system. The recovered yield of 0.34 g/L falls within the range reported for social hymenopteran silk proteins. The purified OligF2 protein pellet was cast into films, with elastic moduli within the range reported for hydrated protein-based films. The ability to produce and process OligF2 recombinantly creates new opportunities to investigate solitary bee silks as tunable recombinant biomaterials and expands the diversity of accessible aculeate silk systems beyond social species. This work provides an initial proof of concept and lays the foundation for systematic exploration of solitary bee silk proteins as a new class of recombinant biomaterials.

Supplementary Materials: The following supporting information can be downloaded at: https://www.mdpi.com/article/10.3390/synbio4020009/s1.

Author Contributions: Conceptualization, O.W., K.K.D., J.J.M., P.E.O., R.V.L. and J.A.J.; methodology, O.W., K.K.D., M.R.W. and E.D.V.N.; formal analysis, O.W. and K.K.D.; investigation, O.W., K.K.D., J.J.M., M.R.W. and B.E.B.; resources, J.A.J.; data curation, O.W., K.K.D., M.R.W., E.D.V.N. and B.E.B.; writing—original draft preparation, O.W. and K.K.D.; writing—review and editing, O.W., K.K.D., P.E.O., B.E.B., R.V.L. and J.A.J.; visualization, K.K.D.; supervision, J.A.J.; project administration, O.W. and J.A.J.; funding acquisition, J.J.M. and J.A.J. All authors have read and agreed to the published version of the manuscript.

Funding: A grant from the Utah State University Office of Research supported this work.

Institutional Review Board Statement: Not applicable.

Informed Consent Statement: Not applicable.

Data Availability Statement: The original contributions presented in this study are included in the article/Supplementary Material. Further inquiries can be directed to the corresponding author.

Acknowledgments: We recognize and appreciate the use of Arizona State University's Eyring Materials Center facilities, supported in part by NNCI-ECCS-2025490.

Conflicts of Interest: The authors declare no conflicts of interest.

Abbreviations

The following abbreviations are used in this manuscript:

DPBS	Dulbecco's phosphate-buffered saline
DTT	dithiothreitol
FTIR-ATR	Fourier-transform infrared attenuated total reflectance
IPA	isopropyl alcohol
IPTG	isopropyl β-D-1-thiogalactopyranoside
OligF2	*Osmia lignaria* silk fibroin 2
PDMS	polydimethylsiloxane
RCF	relative centrifugal force
rHIF	recombinant hagfish intermediate filament
SDS-PAGE	sodium dodecyl sulfate-polyacrylamide gel electrophoresis
TAE	Tris-acetate-EDTA

References

1. Craig, C.L. Evolution of Arthropod Silks. *Annu. Rev. Entomol.* **1997**, *42*, 231–267. [CrossRef] [PubMed]
2. Sutherland, T.D.; Young, J.H.; Weisman, S.; Hayashi, C.Y.; Merritt, D.J. Insect Silk: One Name, Many Materials. *Annu. Rev. Entomol.* **2010**, *55*, 171–188. [CrossRef]
3. Bhattacharyya, G.; Oliveira, P.; Krishnaji, S.T.; Chen, D.; Hinman, M.; Bell, B.; Harris, T.I.; Ghazitabatabaei, A.; Lewis, R.V.; Jones, J.A. Large Scale Production of Synthetic Spider Silk Proteins in *Escherichia coli*. *Protein Expr. Purif.* **2021**, *183*, 105839. [CrossRef] [PubMed]
4. Saric, M.; Scheibel, T. Engineering of Silk Proteins for Materials Applications. *Curr. Opin. Biotechnol.* **2019**, *60*, 213–220. [CrossRef]
5. Dinjaski, N.; Kaplan, D.L. Recombinant Protein Blends: Silk beyond Natural Design. *Curr. Opin. Biotechnol.* **2016**, *39*, 1–7. [CrossRef]
6. Shi, J.; Lua, S.; Du, N.; Liu, X.; Song, J. Identification, Recombinant Production and Structural Characterization of Four Silk Proteins from the Asiatic Honeybee Apis Cerana. *Biomaterials* **2008**, *29*, 2820–2828. [CrossRef]
7. Maitip, J.; Trueman, H.E.; Kaehler, B.D.; Huttley, G.A.; Chantawannakul, P.; Sutherland, T.D. Folding Behavior of Four Silks of Giant Honey Bee Reflects the Evolutionary Conservation of Aculeate Silk Proteins. *Insect Biochem. Mol. Biol.* **2015**, *59*, 72–79. [CrossRef]
8. Weisman, S.; Haritos, V.S.; Church, J.S.; Huson, M.G.; Mudie, S.T.; Rodgers, A.J.W.; Dumsday, G.J.; Sutherland, T.D. Honeybee Silk: Recombinant Protein Production, Assembly and Fiber Spinning. *Biomaterials* **2010**, *31*, 2695–2700. [CrossRef] [PubMed]
9. Kambe, Y.; Sutherland, T.D.; Kameda, T. Recombinant Production and Film Properties of Full-Length Hornet Silk Proteins. *Acta Biomater.* **2014**, *10*, 3590–3598. [CrossRef]
10. Sutherland, T.D.; Church, J.S.; Hu, X.; Huson, M.G.; Kaplan, D.L.; Weisman, S. Single Honeybee Silk Protein Mimics Properties of Multi-Protein Silk. *PLoS ONE* **2011**, *6*, e16489. [CrossRef]
11. Rapson, T.D.; Sutherland, T.D.; Church, J.S.; Trueman, H.E.; Dacres, H.; Trowell, S.C. De Novo Engineering of Solid-State Metalloproteins Using Recombinant Coiled-Coil Silk. *ACS Biomater. Sci. Eng.* **2015**, *1*, 1114–1120. [CrossRef] [PubMed]
12. Huson, M.G.; Church, J.S.; Poole, J.M.; Weisman, S.; Sriskantha, A.; Warden, A.C.; Campbell, P.M.; Ramshaw, J.A.M.; Sutherland, T.D. Controlling the Molecular Structure and Physical Properties of Artificial Honeybee Silk by Heating or by Immersion in Solvents. *PLoS ONE* **2012**, *7*, e52308, Erratum in *PLoS ONE* **2014**, *9*. [CrossRef] [PubMed]
13. Danforth, B.N.; Minckley, R.L.; Neff, J.L.; Fawcett, F. *The Solitary Bees: Biology, Evolution, Conservation*; Princeton University Press: Princeton, NJ, USA, 2019; ISBN 978-0-691-16898-2.
14. Wasserman, O.; Morley, J.J.; Williams, M.-K.F.; Bell, B.E.; Cox-Foster, D.L.; Jones, J.A. An Effective Protocol to Isolate and Mechanically Test Silk Fibers Spun by *Osmia lignaria* Say (Hymenoptera: Megachilidae) Fifth Instar Larvae. *PLoS ONE* **2025**, *20*, e0318918. [CrossRef]
15. Wasserman, O.; Wootton, M.R.; Fairbanks, S.; Bell, B.E.; Williams, M.-K.F.; Jones, J.A. Protocol for Quantifying the Thickness and Puncture Resistance Properties of Solitary Bee Cocoons Using *Osmia lignaria* as a Model. *STAR Protoc.* **2025**, *6*, 104191. [CrossRef]
16. Oliveira, P.E.; Chen, D.; Bell, B.E.; Harris, T.I.; Walker, C.; Zhang, H.; Grob, B.; Lewis, R.V.; Jones, J.A. The next Generation of Protein Super-Fibres: Robust Recombinant Production and Recovery of Hagfish Intermediate Filament Proteins with Fibre Spinning and Mechanical–Structural Characterizations. *Microb. Biotechnol.* **2021**, *14*, 1976–1989. [CrossRef]
17. Wasserman, O.; Oliveira, P.E.; Bell, B.E.; Jefferson, S.; Fairbanks, S.; Watson, A.; Lewis, R.V.; Jones, J.A. Engineered Recombinant Hagfish Intermediate Filament Proteins: Unraveling Domain Roles in Synthetic Fiber Formation and Mechanics. *ACS Omega* **2024**, *9*, 47023–47030. [CrossRef]
18. Bell, B.E.; Burton, I.K.; Arreola-Patino, J.; Harris, T.I.; Oliveira, P.; Chen, D.; Lewis, R.V.; Jones, J.A. Scalable Purification of Recombinant Structural Proteins, Hagfish Intermediate Filament α and γ, from Inclusion Bodies for Fiber Formation. *Protein Expr. Purif.* **2022**, *199*, 106152. [CrossRef]
19. Wang, R.; Dai, X.; Zhao, S.; Yin, Z.; Su, L.; Wang, C.; Chen, H.; Zheng, L.; Liu, Y.; Zhai, Y. Chromosomal-Level Genome Assembly of Solitary Bee Pollinator *Osmia excavata* Alfken (Hymenoptera: Megachilidae). *Sci. Data* **2025**, *12*, 908. [CrossRef] [PubMed]
20. Santos, P.K.F.; de Souza Araujo, N.; Françoso, E.; Werren, J.H.; Kapheim, K.M.; Arias, M.C. The Genome of the Solitary Bee *Tetrapedia diversipes* (Hymenoptera, Apidae). *G3 Genes Genomes Genet.* **2025**, *15*, jkae264. [CrossRef]
21. Nash, W.J.; Man, A.; McTaggart, S.; Baker, K.; Barker, T.; Catchpole, L.; Durrant, A.; Gharbi, K.; Irish, N.; Kaithakottil, G.; et al. The Genome Sequence of the Violet Carpenter Bee, *Xylocopa violacea* (Linnaeus, 1785): A Hymenopteran Species Undergoing Range Expansion. *Heredity* **2024**, *133*, 381–387. [CrossRef]
22. Beadle, K.; Singh, K.S.; Troczka, B.J.; Randall, E.; Zaworra, M.; Zimmer, C.T.; Hayward, A.; Reid, R.; Kor, L.; Kohler, M.; et al. Genomic Insights into Neonicotinoid Sensitivity in the Solitary Bee *Osmia bicornis*. *PLoS Genet.* **2019**, *15*, e1007903. [CrossRef]
23. Walsh, A.T.; Triant, D.A.; Le Tourneau, J.J.; Shamimuzzaman, M.; Elsik, C.G. Hymenoptera Genome Database: New Genomes and Annotation Datasets for Improved Go Enrichment and Orthologue Analyses. *Nucleic Acids Res.* **2022**, *50*, D1032–D1039. [CrossRef] [PubMed]

24. Stolle, E.; Guiglielmoni, N.; Kirangwa, J.; Kukowka, S.; Meitzel, T.; Cartney, A.M.M.; Heilmann-Heimbach, S.; Becker, K.; Köhrer, K.; Böhne, A. Reference Genome Sequence of the Solitary Bee *Camptopoeum friesei* Mocsáry, 1894 (Hymenoptera, Andrenidae). *arXiv* **2023**, arXiv:2023.08.27.555015.
25. Rickabaugh, E.; Weatherston, D.; Harris, T.I.; Jones, J.A.; Vargis, E. Engineering a Biomimetic In Vitro Model of Bruch's Membrane Using Hagfish Slime Intermediate Filament Proteins. *ACS Biomater. Sci. Eng.* **2023**, *9*, 5051–5061. [CrossRef] [PubMed]
26. Mello, M.L.S.; dos Anjos, E.H.M.; de Campos Vidal, B.; Rozen, J.G. Topochemistry, Optical Anisotropy and FT-IR Microspectroscopy of the Cocoon of *Lithurgus chrysurus* (Hymenoptera, Megachilidae). *Micron* **2016**, *90*, 87–96. [CrossRef] [PubMed]
27. Heimburg, T.; Schünemann, J.; Weber, K.; Geisler, N. FTIR-Spectroscopy of Multistranded Coiled Coil Proteins. *Biochemistry* **1999**, *38*, 12727–12734. [CrossRef]
28. Hu, X.; Kaplan, D.; Cebe, P. Dynamic Protein−Water Relationships during β-Sheet Formation. *Macromolecules* **2008**, *41*, 3939–3948. [CrossRef]
29. Hu, X.; Kaplan, D.; Cebe, P. Determining Beta-Sheet Crystallinity in Fibrous Proteins by Thermal Analysis and Infrared Spectroscopy. *Macromolecules* **2006**, *39*, 6161–6170. [CrossRef]
30. Teramoto, H.; Miyazawa, M. Analysis of Structural Properties and Formation of Sericin Fiber by Infrared Spectroscopy. *J. Insect Biotechnol. Sericol.* **2003**, *72*, 157–162. [CrossRef]
31. Shilling, P.J.; Pontes-Braz, L.; Mitchell, L.; Howell, L.; Veneer, P.; Jayashree, S.; Castelli, L.A.; Pham, T.; Lu, L.; Wang, B.; et al. Production of Recombinant Coiled Coil Silk Proteins for Materials Synthesis. *Protein Expr. Purif.* **2025**, *229*, 106683. [CrossRef]
32. Sutherland, T.D.; Weisman, S.; Walker, A.A.; Mudie, S.T. Invited Review: The Coiled Coil Silk of Bees, Ants, and Hornets. *Biopolymers* **2012**, *97*, 446–454. [CrossRef] [PubMed]
33. Campbell, P.M.; Trueman, H.E.; Zhang, Q.; Kojima, K.; Kameda, T.; Sutherland, T.D. Cross-Linking in the Silks of Bees, Ants and Hornets. *Insect Biochem. Mol. Biol.* **2014**, *48*, 40–50. [CrossRef]
34. Sutherland, T.D.; Campbell, P.M.; Weisman, S.; Trueman, H.E.; Sriskantha, A.; Wanjura, W.J.; Haritos, V.S. A Highly Divergent Gene Cluster in Honey Bees Encodes a Novel Silk Family. *Genome Res.* **2006**, *16*, 1414–1421. [CrossRef]
35. Johnston, C.L.; Jobichen, C.; Briggs, L.J.; Michie, M.; Liu, J.; Morton, C.J.; Warden, A.C.; Sutherland, T.D. Resolving the Structure and Assembly of the Honeybee Silk Heterotetrameric Coiled Coil. *Protein Sci.* **2025**, *34*, e70230. [CrossRef]
36. Byler, D.M.; Susi, H. Examination of the Secondary Structure of Proteins by Deconvolved FTIR Spectra. *Biopolymers* **1986**, *25*, 469–487. [CrossRef]
37. Heimburg, T.; Schuenemann, J.; Weber, K.; Geisler, N. Specific Recognition of Coiled Coils by Infrared Spectroscopy: Analysis of the Three Structural Domains of Type III Intermediate Filament Proteins. *Biochemistry* **1996**, *35*, 1375–1382. [CrossRef]
38. Fang, G.; Huang, Y.; Tang, Y.; Qi, Z.; Yao, J.; Shao, Z.; Chen, X. Insights into Silk Formation Process: Correlation of Mechanical Properties and Structural Evolution during Artificial Spinning of Silk Fibers. *ACS Biomater. Sci. Eng.* **2016**, *2*, 1992–2000. [CrossRef] [PubMed]
39. Lawrence, B.D.; Wharram, S.; Kluge, J.A.; Leisk, G.G.; Omenetto, F.G.; Rosenblatt, M.I.; Kaplan, D.L. Effect of Hydration on Silk Film Material Properties. *Macromol. Biosci.* **2010**, *10*, 393–403. [CrossRef]
40. Gopalakrishnan, S.; Xu, J.; Zhong, F.; Rotello, V.M. Strategies for Fabricating Protein Films for Biomaterial Applications. *Adv. Sustain. Syst.* **2021**, *5*, 2000167. [CrossRef] [PubMed]
41. Chan, W.H.; Hussain, A.A.; Marshall, J. Youngs Modulus of Bruchs Membrane: Implications for AMD. *Investig. Ophthalmol. Vis. Sci.* **2007**, *48*, 2187.
42. Curcio, C.A.; Johnson, M. Structure, Function, and Pathology of Bruch's Membrane. In *Retina*; Elsevier: Amsterdam, The Netherlands, 2013; pp. 465–481; ISBN 978-1-4557-0737-9.

Disclaimer/Publisher's Note: The statements, opinions and data contained in all publications are solely those of the individual author(s) and contributor(s) and not of MDPI and/or the editor(s). MDPI and/or the editor(s) disclaim responsibility for any injury to people or property resulting from any ideas, methods, instructions or products referred to in the content.